Research Article | Vol. 9, No. 12 | 1 Dec 2018 | BIOMEDICAL OPTICS EXPRESS 6350
Biomedical Optics EXPRESS

Polarization-resolved second harmonic microscopy of skeletal muscle in sepsis

MATTHIEU DUBREUIL,[1,*] FLORINE TISSIER,[2] LUCAS LE ROY,[2] JEAN-PIERRE PENNEC,[2] SYLVAIN RIVET,[1] MARIE-AGNÈS GIROUX-METGES,[2] AND YANN LE GRAND[1]

[1]*Université de Bretagne Occidentale, Laboratoire d'optique et de magnétisme OPTIMAG EA 938, IBSAM, 6 avenue Le Gorgeu, Brest, 29238, France*
[2]*Université de Bretagne Occidentale, Laboratoire optimisation des régulations physiologiques ORPHY EA 4324, IBSAM, 6 avenue Le Gorgeu, Brest, 29238, France*
**matthieu.dubreuil@univ-brest.fr*

Abstract: Polarization-resolved second harmonic generation (P-SHG) microscopy is able to probe the sub-micrometer structural organization of myosin filaments within skeletal muscle. In this study, P-SHG microscopy was used to analyze the structural consequences of sepsis, which is the main cause of the critical illness polyneuromyopathy (CIPNM). Experiments conducted on two populations of rats demonstrated a significant difference of the anisotropy parameter between healthy and septic groups, indicating that P-SHG microscopy is promising for the diagnosis of CIPNM. The difference, which can be attributed to a change of myosin conformation at the sub-sarcomere scale, cannot be evidenced by classical SHG imaging.

1. Introduction

Among muscle pathologies, critical illness polyneuromyopathy (CIPNM) [1] affects roughly 30% of patients in intensive care units (ICU) and is composed of many heterogeneous disorders that lead to muscle weakness and failure from weaning of mechanical ventilation. Sepsis is an inappropriate systemic inflammatory response syndrome, associated with infection. It could lead to dysfunction of multiple organ including striated muscles. Sepsis is one of the main causes of neuromyopathy acquired in ICU and can lead to long-term sequelae at the muscular level. There is an early prognosis with increased morbidity and cost of hospitalization [2] but also deaths from acute respiratory failure [3]. There is also a late prognosis with sometimes significant sequelae up to a locomotor deficit impacting the quality of life [4] and may persist for several years after the healing of the initial pathology. The pathophysiology of neuromyopathy acquired in ICU is complex and incompletely known. Chronic sepsis has been shown to induce changes in the mechanical characteristics of the muscle with in particular, a decrease in active force and an increase in passive force [5]. This could be due to modifications of protein expression or phosphorylation, disorganization of myofibrils and/or residual interactions between contractile proteins (actin, myosin). Currently, consequences of sepsis on the structural organization of muscular proteins at the microscopic and sub-microscopic scale are difficult to investigate with classical biological methods [6].

Second harmonic generation (SHG) microscopy [7] is a laser scanning technique used as a powerful tool for label-free *ex vivo* or *in vivo* imaging of fibrous proteins such as collagen and myosin [8]. SHG is highly sensitive to the microscopic and mesoscopic orders of these noncentrosymmetric supramolecular arrangements and also to their orientations with respect to the polarization of the excitation laser beam. Knowledge of the polarization-resolved second harmonic generation (P-SHG) response of such molecular assemblies provides additional information that can be used to reveal geometrical details up to the molecular level scale [9–13]. Typically the anisotropy parameter ρ, defined as the ratio χ_{zzz}/χ_{zxx} between the two principal components of the $\chi^{(2)}$-tensor of collagen and myosin, and associated to the

#346689 https://doi.org/10.1364/BOE.9.006350
Journal © 2018 Received 24 Sep 2018; revised 7 Nov 2018; accepted 11 Nov 2018; published 19 Nov 2018

Biomedical Optics EXPRESS

geometrical distribution of second harmonic emitters within the focal volume [9–11], is deduced from P-SHG experiments. In muscle, it was shown that the anisotropy parameter ρ could be convenient to detect structural organization of myosin within the sarcomeres [14–16]. Modifications of myosin conformation are probably at the origin of some functional changes observed in the case of sepsis [17], for example the increase of the passive force and decrease of active force on a fast muscle like the *Extensor Digitorum Longus* (EDL).

Although several P-SHG experiments were conducted to investigate the microstructure of myosin filaments within muscle [10,13–16,18–20], few of these studies take place in the context of specific muscle pathology and none in the case of sepsis-induced polyneuromyopathy. In this article, we present results of P-SHG experiments conducted over a large set of optical sections made of rat EDL muscles taken from two populations, one healthy and the other afflicted by chronic sepsis.

2. Material and methods

2.1 Animal samples

A process of chronic sepsis induction by caecal ligation-perforation in the rat was used [5,6]. Fourteen 3 months-old female Wistar rats were sacrificed in respect with the local committee of ethic protocol (authorization n°02076.01) and divided into 2 groups (control and septic) composed of 7 animals each. Rats of the control group underwent the same operation as the septic group but without ligation and caecal perforation. Rats were sacrificed 7 days after operation, enabling to qualify the sepsis as chronic. EDL muscles were removed from right and left hind limb, fixed in 4% paraformaldehyde at the resting length and embedded in OCT compound. Histological slices of 10µm thickness were produced by a cryotom in the longitudinal direction of muscles in order to form optical sections of ~1x0.2cm^2 for imaging under the P-SHG microscope. Two optical sections per muscle were realized, resulting in 4 optical sections per specimen (right and left hind limb), *i.e.* 28 optical sections per group.

2.2 Microscopy setup

The experimental setup is depicted in Fig. 1 and consists of a laser scanning unit (FV300, Olympus) mounted on an upright microscope (BX51WI, Olympus). The light source is a horizontally polarized Ti:Sapphire laser (Verdi-V5/Mira900F, Coherent) tuned at 830nm for all experiments and attenuated with a 0.6ND neutral density filter to avoid degradation of the samples. Light was focused on the sample by a 20X/0.75NA microscope objective (UPlanSApo, Olympus), resulting in experimental lateral and axial resolutions (FWHM) of respectively ~0.5µm and ~1.7µm, measured with fluorescent microspheres (Polybead polystyrene red dyed microsphere 0.20µm, PolySciences Inc.). A 60mW optical power was measured at the sample plane with a microscope slide thermal sensor (S175C, Thorlabs). Second harmonic light was collected in the forward direction by a 0.7NA condenser and detected through a 415/10nm FWHM bandpass filter by an external analog PMT module (H10721-210, Hamamatsu) whose voltage was adjusted to optimize signal to noise ratio while avoiding saturation of pixels. SHG images were acquired with 12-bit intensity resolution and 1024x1024 pixel^2 definition. The pixel dwell-time was about 8µs and a 5-time zoom was used resulting in a 142x142µm^2 field of view for the images.

P-SHG images were obtained according to the method proposed in [13]. Four P-SHG images were sequentially acquired, corresponding to 4 linearly polarized states of the excitation laser beam (0°, 45°, 90° and 135° with respect to the horizontal image side) produced by a zero-order half-wave quartz plate (25.4mm diameter, 830.0nm λ/2, Edmunds Optics) mounted in a motorized rotating stage (PR50CC, Newport) and set just above the entrance pupil of the microscope objective. The polarization extinction ratio of the fundamental laser beam was measured at the sample plane using the microscope slide thermal sensor and a high acceptance angle polarizer (ColorPol VIS-IR polarizer, Codixx). The

Biomedical Optics EXPRESS

extinction ratio was very close for all input polarizations with a value of 180:1 which means 4.2° residual ellipticity. We developed a custom LabView program (National Instruments) to control and synchronize the 4 images acquisition sequence with the corresponding 4 input polarization states.

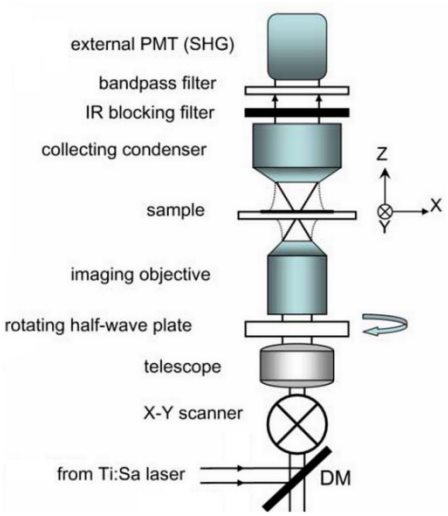

Fig. 1. Experimental microscope setup. See text for details about optical elements.

2.3 Sarcomere length and anisotropy parameter measurement

Sarcomere length (SL) and anisotropy parameter ρ were calculated using custom Matlab software (Matlab R2010a, Mathworks).

First, isotropic SHG image, equivalent to SHG image obtained under circular polarization excitation, was reconstructed from the sum of the 4 P-SHG images [13,20]. The regular arrangement of sarcomeres within myofibrils can be evidenced by the typical striated pattern observed in SHG imaging (Fig. 2(a)).

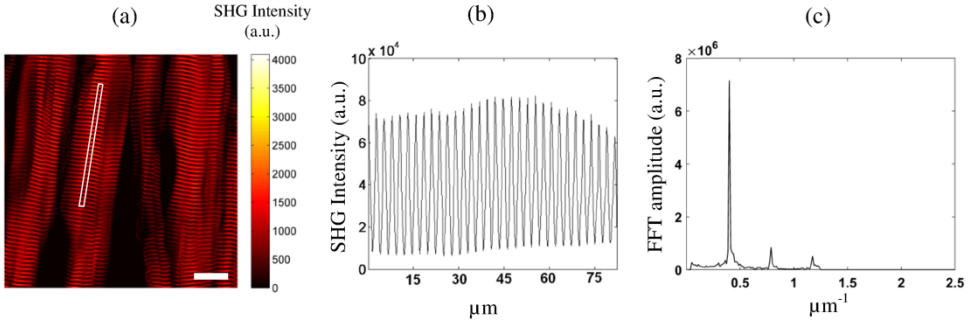

Fig. 2. Determination of the sarcomere length. (a) Isotropic SHG image reconstructed from the 4 P-SHG images with the 4 input polarizations. The white rectangle highlights the ROI used for the determination of the sarcomere length. (b) Intensity plot profile of the ROI after rotation and binning. (c) Fourier transformation of the intensity plot profile. The sarcomere length is calculated from the maximum value of the peak at the lowest frequency. Scale bar 20µm.

The process used to extract the sarcomere length consisted in: 1/ selecting a region of interest (ROI) containing ~20-30 sarcomeres within a given myofibril (Fig. 2(a)), 2/ performing a 2D fast fourier transform (fft) of the ROI and searching for the position of the maximum to find the direction of the myofibril, 3/ rotating the ROI to align the myofibril

Biomedical Optics EXPRESS

horizontally, 4/ applying a vertical binning to reduce noise and generating a 1D intensity plot profile along the myofibril (Fig. 2(b)), 5/ performing a 1D fft of the intensity plot profile and evaluating the sarcomere length from the maximum value of the lowest frequency peak (Fig. 2(c)). The sarcomere length was evaluated for different ROIs selected within a single image in order to check for the repeatability and robustness of the measurement method. The typical dispersion of values was found to be around 0.05µm (standard deviation over 10 measurements) for a mean value of 2.45µm, which means less than 2% dispersion for a single image.

The 4 P-SHG images were processed according to the method proposed in [13] to extract the anisotropy parameter ρ for each pixel (Fig. 3).

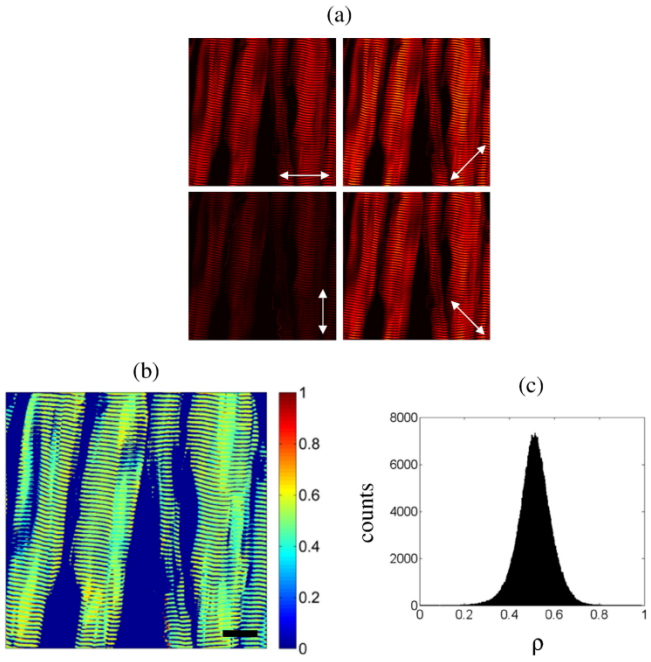

Fig. 3. Measurement of the anisotropy parameter ρ. Same specimen as in Fig. 2. (a) Four P-SHG images corresponding to 4 input linear polarizations (0°, 45°, 90° and 135° with respect to horizontal image side). (b) Pixel map of anisotropy parameter ρ and (c) histogram of ρ. Scale bar 20µm.

As demonstrated in [13], SHG intensity can be expressed as:

$$I^{SHG}(\psi) = U + V\cos(2\psi - 2\phi) + W\cos(4\psi - 4\phi) \qquad (1)$$

where ψ is the input polarization angle, ϕ the orientation of the axis of cylindrical symmetry, and U, V, and W real quantities depending on the anisotropy parameter ρ. It is possible, with only 4 acquisitions corresponding to 4 input linear polarizations (0°, 45°, 90° and 135°) and simple arithmetic operations to extract the anisotropy parameter ρ. It was assumed, as usual, that myosin filaments can be described by rod shaped supramolecules of cylindrical C_∞ symmetry with a dominant hyperpolarizability coefficient β, and that Kleinman symmetry conditions are fulfilled. It was also assumed that the anisotropy parameter $\rho<1$ to remove any ambiguity of the method using only 4 input polarizations. This latter assumption is reasonable according to the typical experimental values of anisotropy parameter found in the literature for myosin in skeletal muscle of mammalians, ranging from ~0.3 to ~0.8 depending on the physiological state and the animal. We point out that anisotropy parameter determination usually suffers from small systematic errors of the instrument that comes from high NA

Biomedical Optics EXPRESS

focusing [21] or residual ellipticity of input polarizations [9]. In this study, the use of a 0.75NA objective enables to neglect the influence of high NA focusing, polarizations mixing becoming sensitive from NA = 0.8 [9,22]. Then, the influence of residual ellipticity was evaluated by simulations and was found to be almost negligible with this method (less than 1% deviation on the value of ρ for ρ = 0.6 with 5% residual ellipticity).

The 4 input polarization method used here is very straightforward to implement and benefits from reduced acquisition time as compared to traditional methods based on more than 10 acquisition frames. Background noise was subtracted and pixels whose SHG intensity (calculated from isotropic SHG images) was below 10% of the full dynamic range were not processed for the calculation of ρ in order to exclude parts of myofibrils that are not in-plane. The repeatability on the determination of ρ was evaluated by performing 10 successive measurements on a given specimen. The variability of ρ for a selected pixel was found to be less than 1%, giving insight into the precision on the determination of ρ by our setup and method. For comparison between the two populations of rats, the mean value of ρ over all processed pixel was calculated for each pixel map. A pixel map of the anisotropy parameter [24] for a typical specimen is presented in Fig. 3(b) and the corresponding ρ-values histogram in Fig. 3(c). It can be noticed that the variability of anisotropy parameter for a given specimen (around 10%, see Fig. 3(c)) is well above the precision of the instrument (around 1%).

2.4 Statistical analysis

For each optical section of size ~1x0.2cm^2, 3 distinct areas (142x142µm^2) were imaged, which corresponds to 2 to 5 myofibrils depending on the optical section. The mean value of ρ, calculated over all significant pixels (10% threshold), was determined for each image. The mean sarcomere length was also determined for each image. This gives 4x3 = 12 values of SL and ρ per specimen, and 28x3 = 84 values of SL and ρ per group of specimens. Results were represented as statistical box plots (Fig. 4(a) for SL and Fig. 4(d) for ρ) where the whiskers represent extremal values, the boxes represent the 25-75 percentiles and the filled squares indicate the mean value of the population. A Mann-Whitney non-parametric test was used to assess the statistical difference ($p < 0.05$) between the two populations.

3. Results

A loss of muscular weight (20-25%) was observed for rats of the septic group in the lateral and medial *gastrocnemius*, which validates the presence of sepsis [17]. The comparison of SL between control and septic specimens is presented in Fig. 4(a) as statistical box plot. Representative isotropic SHG images of a healthy and a septic specimen are displayed in Fig. 4(b) and Fig. 4(c), respectively. Sarcomere lengths are comparable with the values found in the literature for skeletal muscle of mammalians (1.2-2.4µm in [10] for mouse, 2.4-4.4µm in [15] for rabbits, 2.0µm in [25] for rats, 1.6-2.0µm in [26] for mice). No statistical difference ($p>0.1$) can be evidenced between control (2.39 ± 0.23µm) and septic (2.44 ± 0.22µm) groups according to the mean sarcomere length, suggesting that sepsis does not affect the regular organization of striated muscle at this scale. No obvious degradation of sarcomeres and no contraction or stretching of EDL muscles were evidenced by classical SHG imaging in these experiments.

The comparison of ρ between control and septic specimens is presented in Fig. 4(d). Representative anisotropy parameter pixel maps of a healthy and a septic specimen are displayed in Fig. 4(e) and Fig. 4(f), respectively. Anisotropy parameter values lie in the range of values found in the literature for skeletal muscle of mammalians (0.5-0.6 in [13], 0.50-0.73 in [14], 0.46-0.68 in [15], 0.54-0.70 in [16], 0.29-0.52 in [30]). The experiments demonstrate a statistical difference ($p<0.001$) between control (0.575 ± 0.036) and septic (0.499 ± 0.050) groups according to the mean anisotropy parameter, which is significantly lower in the septic group than in the control group. This result first indicates that anisotropy parameter can be considered as a discriminating parameter to distinguish between control and septic specimens,

Biomedical Optics EXPRESS

in view to evaluation and diagnosis of CIPNM induced by sepsis. This result also suggests an alteration of muscle structure at the sub-sarcomere scale at first stage of sepsis, which cannot be evidenced by classical intensity-based SHG imaging. This alteration can be explained by a modification of myosin conformation and/or organization as detailed in the discussion.

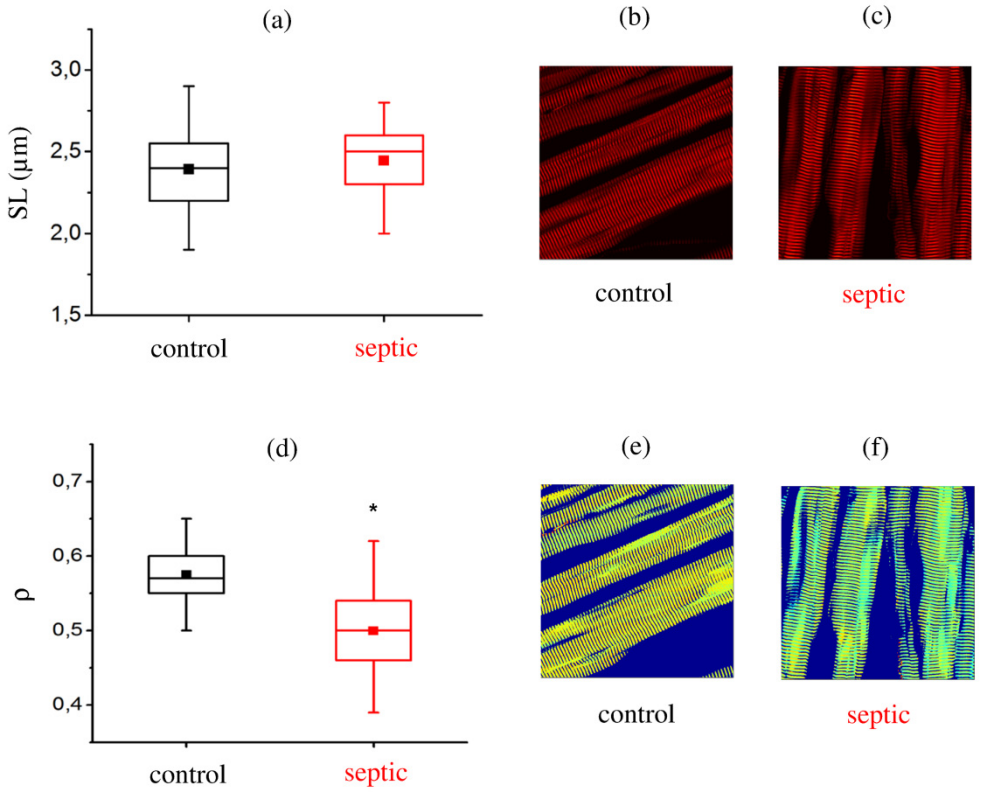

Fig. 4. Comparison of (a) sarcomere length (SL) and (d) anisotropy parameter ρ between control and septic groups. Representative isotropic SHG images (b,c) and anisotropy parameter pixel maps (e,f) of a control (b,e) and a septic (c,f) specimen, with the same colormap range as in Fig. 3. * $p < 0.001$.

4. Discussion

In P-SHG experiments, anisotropy parameter is sensitive to the structural distribution of hyper Rayleigh scattering (HRS) emitters within the focal excitation volume of the microscope objective [9]. However, relationship between the distribution of HRS emitters and anisotropy parameter is highly underdetermined because many different distributions of HRS emitters can lead to the same value of ρ. Myosin thick filaments are composed of a juxtaposition of long polypeptide α-helices, elementary HRS emitters lying in C-N bonds of amide groups [10]. All HRS emitters are almost planar and tilted at a fixed polar angle with respect to the helical axis. Moreover, myosin has a particular geometrical structure because in addition to the static thick filament, it is also composed of a dynamic part made of two-heads supported by a coiled coil rod-like structure that links myosin heads to the thick filament. In the case of myosin, one can reasonably assume that modification of anisotropy parameter can have three origins. The first possibility is a modification of the α–helix pitch angle, assuming a perfectly planar and parallel organization between α-helices and no contribution to SHG of the dynamic part of myosin [13,16]. The second possibility is a reorganization of α-helices leading to a change of their orientation distribution and thus of the HRS emitters orientation

Biomedical Optics EXPRESS

distribution, as already established for collagen [23]. The last possibility is a modification of the conformation of myosin heads [14,15]. Indeed, it was interestingly established in [15] that a non-negligible part of SHG in fact originates from the dynamic part, enabling P-SHG to probe several physiological states of myosin, particularly the fraction of myosin heads attached to actin, also called cross-bridges.

At this stage, it is not possible to fully assess the origin of the decrease of the anisotropy parameter, but we can try to link this observation with some biological processes proposed in the case of sepsis. Firstly, a decrease of anisotropy parameter could indicate an increase of the α–helix pitch angle of myosin [13,16]. It was established [27,28] that sepsis could induce a transformation of muscle fibers of type 2 (medium and large diameter) into muscle fibers of type 1 (small diameter). This transformation is consistent with the decrease of active force and is supported by the diminution of myofibrils diameter observed for septic specimens [17]. As each type of muscle fiber involves a particular isoform of myosin, the microscopic difference between the two isoforms could lie in their α–helix pitch angle. This interpretation has to be confirmed by P-SHG experiments on isolated myosin fibrils of each isoform. Secondly, the decrease of the anisotropy parameter could be induced by a broadening of myosin α-helices orientations. Sepsis is characterized by a degradation of contractile and regulatory myofilament proteins, mostly titin and desmin, as a result of both increased proteolysis and decreased transcription [27]. Myosin is also degraded and its degradation could manifest as a disorganization of α-helices at the sub-sarcomere scale. Finally, a decrease of anisotropy parameter could indicate a diminution of the number residual cross-bridges at rest [15]. Although this interpretation is not consistent with the increase of passive force observed on septic rats, which would suggest on the contrary an increase of residual cross-bridges [29], this could be explained by an alteration of troponin or tropomyosin, which rule the formation of cross-bridges. Indeed, an important decrease of protein expression and particularly of tropomyosin concentration was shown to be induced by sepsis in rapid and slow muscle fibers, releasing binding sites of myosin heads on actin [27]. Nevertheless, increase in passive force could also be related to modifications in other proteins such as titin, masking an effect on cross-bridges.

In order to go further into the understanding of microstructural organization of myofilaments and the consequences of sepsis, dynamic experiments will have to be carried out. Determination of the anisotropy parameter at rest, at full contraction and during contraction should enable to better analyze the behavior of actin/myosin complex and its alteration by sepsis. Currently, most of P-SHG techniques suffer from a lack of temporal resolution, preventing from imaging large areas at sufficient speed. Efforts need to be done in this direction [30], as already engaged by our team [31]. In addition, analyzing both forward and backward P-SHG will help to get better insight into the spatial distribution of HRS emitters and thus the structural organization of myosin [32]. Finally, turning these experiments to clinical conditions should benefits from recent advances in nonlinear endomicroscopy [33]. However, P-SHG experiments conducted *in vivo* on thick intact muscle fibers will have to cope with strong backscattering of second harmonic light [32] and care should be taken to obtain a good discrimination of septic specimens according to the anisotropy parameter in these conditions. Backward P-SHG experiments on histological slices and thick intact muscle fibers of septic and control specimens are currently in progress.

5. Summary

In this study, a significant difference was highlighted between control and septic specimens according to the P-SHG anisotropy parameter ρ, indicating that P-SHG is promising for diagnosis of CIPNM and possibly long term sequelae prediction. Classical SHG images of the striated muscle pattern do not suggest any significant and observable difference between the two groups according to the regularity of the sarcomeres, suggesting a modification of myosin conformation/organization at the sub-micrometer scale. These results could help to better

Biomedical Optics EXPRESS

understand microscopic structural effects of neuromyopathy acquired in ICU. More generally and in the longer term, in addition with the classical advantages conferred by SHG microscopy (optical sectioning, label-free,...), P-SHG holds great promise for the development of biomedical technology for clinical diagnosis of muscular pathologies involving alteration of sub-micrometric structures within the sarcomere.

Funding

IBSAM (Institut Brestois Santé Agro Matière).

Disclosures

The authors declare that there are no conflicts of interest related to this article.

References

1. S. J. Bird and M. M. Rich, "Critical illness myopathy and polyneuropathy," Curr. Neurol. Neurosci. Rep. **2**(6), 527–533 (2002).
2. J. Garnacho-Montero, R. Amaya-Villar, J. L. García-Garmendía, J. Madrazo-Osuna, and C. Ortiz-Leyba, "Effect of critical illness polyneuropathy on the withdrawal from mechanical ventilation and the length of stay in septic patients," Crit. Care Med. **33**(2), 349–354 (2005).
3. D. Intiso, L. Amoruso, M. Zarrelli, L. Pazienza, M. Basciani, G. Grimaldi, A. Iarossi, and F. Di Rienzo, "Long-term functional outcome and health status of patients with critical illness polyneuromyopathy," Acta Neurol. Scand. **123**(3), 211–219 (2011).
4. L. H. Visser, "Critical illness polyneuropathy and myopathy: clinical features, risk factors and prognosis," Eur. J. Neurol. **13**(11), 1203–1212 (2006).
5. B. Rossignol, G. Gueret, J. P. Pennec, J. Morel, F. Rannou, M. A. Giroux-Metges, H. Talarmin, M. Gioux, and C. C. Arvieux, "Effects of chronic sepsis on contractile properties of fast twitch muscle in an experimental model of critical illness neuromyopathy in the rat," Crit. Care Med. **36**(6), 1855–1863 (2008).
6. B. Rossignol, G. Gueret, J. P. Pennec, J. Morel, M. A. Giroux-Metges, H. Talarmin, and C. C. Arvieux, "Effects of chronic sepsis on the voltage-gated sodium channel in isolated rat muscle fibers," Crit. Care Med. **35**(2), 351–357 (2007).
7. F. S. Pavone and P. J. Campagnola, *Second Harmonic Generation Imaging*, Series in cellular and clinical imaging (CRC Press, 2014).
8. P. J. Campagnola and L. M. Loew, "Second-harmonic imaging microscopy for visualizing biomolecular arrays in cells, tissues and organisms," Nat. Biotechnol. **21**(11), 1356–1360 (2003).
9. S. Brasselet, "Polarization-resolved nonlinear microscopy: application to structural molecular and biological imaging," Adv. Opt. Photonics **3**(3), 205 (2011).
10. S. V. Plotnikov, A. C. Millard, P. J. Campagnola, and W. A. Mohler, "Characterization of the Myosin-Based Source for Second-Harmonic Generation from Muscle Sarcomeres," Biophys. J. **90**(2), 693–703 (2006).
11. A. E. Tuer, M. K. Akens, S. Krouglov, D. Sandkuijl, B. C. Wilson, C. M. Whyne, and V. Barzda, "Hierarchical Model of Fibrillar Collagen Organization for Interpreting the Second-Order Susceptibility Tensors in Biological Tissue," Biophys. J. **103**(10), 2093–2105 (2012).
12. P. Stoller, B. M. Kim, A. M. Rubenchik, K. M. Reiser, and L. B. Da Silva, "Polarization-dependent optical second-harmonic imaging of a rat-tail tendon," J. Biomed. Opt. **7**(2), 205–214 (2002).
13. C. Odin, T. Guilbert, A. Alkilani, O. P. Boryskina, V. Fleury, and Y. Le Grand, "Collagen and myosin characterization by orientation field second harmonic microscopy," Opt. Express **16**(20), 16151–16165 (2008).
14. S. Schürmann, F. von Wegner, R. H. Fink, O. Friedrich, and M. Vogel, "Second harmonic generation microscopy probes different states of motor protein interaction in myofibrils," Biophys. J. **99**(6), 1842–1851 (2010).
15. V. Nucciotti, C. Stringari, L. Sacconi, F. Vanzi, L. Fusi, M. Linari, G. Piazzesi, V. Lombardi, and F. S. Pavone, "Probing myosin structural conformation in vivo by second-harmonic generation microscopy," Proc. Natl. Acad. Sci. U.S.A. **107**(17), 7763–7768 (2010).
16. F. Tiaho, G. Recher, and D. Rouède, "Estimation of helical angles of myosin and collagen by second harmonic generation imaging microscopy," Opt. Express **15**(19), 12286–12295 (2007).
17. R. Stevens, *et al*., *Textbook of Post-ICU Medicine: The Legacy of Critical Care* (Oxford University Press, 2014).
18. L. Kontenis, M. Samim, A. Karunendiran, S. Krouglov, B. Stewart, and V. Barzda, "Second harmonic generation double stokes Mueller polarimetric microscopy of myofilaments," Biomed. Opt. Express **7**(2), 559–569 (2016).
19. O. Nadiarnykh and P. J. Campagnola, "Retention of polarization signatures in SHG microscopy of scattering tissues through optical clearing," Opt. Express **17**(7), 5794–5806 (2009).
20. C. Odin, Y. Le Grand, A. Renault, L. Gailhouste, and G. Baffet, "Orientation fields of nonlinear biological fibrils by second harmonic generation microscopy," J. Microsc. **229**(1), 32–38 (2008).
21. E. Yew and C. Sheppard, "Effects of axial field components on second harmonic generation microscopy," Opt. Express **14**(3), 1167–1174 (2006).

Biomedical Optics EXPRESS

22. P. Schön, M. Behrndt, D. Aït-Belkacem, H. Rigneault, and S. Brasselet, "Polarization and phase pulse shaping applied to structural contrast in nonlinear microscopy imaging," Phys. Rev. A **81**(1), 013809 (2010).
23. D. Rouède, E. Schaub, J. J. Bellanger, F. Ezan, J. C. Scimeca, G. Baffet, and F. Tiaho, "Determination of extracellular matrix collagen fibril architectures and pathological remodeling by polarization dependent second harmonic microscopy," Sci. Rep. **7**(1), 12197 (2017).
24. S. Psilodimitrakopoulos, D. Artigas, G. Soria, I. Amat-Roldan, A. M. Planas, and P. Loza-Alvarez, "Quantitative discrimination between endogenous SHG sources in mammalian tissue, based on their polarization response," Opt. Express **17**(12), 10168–10176 (2009).
25. G. Recher, D. Rouède, P. Richard, A. Simon, J. J. Bellanger, and F. Tiaho, "Three distinct sarcomeric patterns of skeletal muscle revealed by SHG and TPEF microscopy," Opt. Express **17**(22), 19763–19777 (2009).
26. S. V. Plotnikov, A. M. Kenny, S. J. Walsh, B. Zubrowski, C. Joseph, V. L. Scranton, G. A. Kuchel, D. Dauser, M. Xu, C. C. Pilbeam, D. J. Adams, R. P. Dougherty, P. J. Campagnola, and W. A. Mohler, "Measurement of muscle disease by quantitative second-harmonic generation imaging," J. Biomed. Opt. **13**(4), 044018 (2008).
27. S. Hussain, *et al*., "Differential regulation of skeletal muscle myofilament protein expression in sepsis," Eur. Respir. J. **50**(61), OA301 (2017).
28. R. Billeter, C. W. Heizmann, H. Howald, and E. Jenny, "Analysis of myosin light and heavy chain types in single human skeletal muscle fibers," Eur. J. Biochem. **116**(2), 389–395 (1981).
29. V. Joumaa, D. E. Rassier, T. R. Leonard, and W. Herzog, "The origin of passive force enhancement in skeletal muscle," Am. J. Physiol. Cell Physiol. **294**(1), C74–C78 (2008).
30. S. Psilodimitrakopoulos, P. Loza-Alvarez, and D. Artigas, "Fast monitoring of in-vivo conformational changes in myosin using single scan polarization-SHG microscopy," Biomed. Opt. Express **5**(12), 4362–4373 (2014).
31. M. Dubreuil, S. Rivet, and Y. Le Grand, "Snapshot second-harmonic generation polarimeter based on spectral analysis," Opt. Lett. **42**(22), 4639–4642 (2017).
32. F. Légaré, C. Pfeffer, and B. R. Olsen, "The Role of Backscattering in SHG Tissue Imaging," Biophys. J. **93**(4), 1312–1320 (2007).
33. G. Ducourthial, P. Leclerc, T. Mansuryan, M. Fabert, J. Brevier, R. Habert, F. Braud, R. Batrin, C. Vever-Bizet, G. Bourg-Heckly, L. Thiberville, A. Druilhe, A. Kudlinski, and F. Louradour, "Development of a real-time flexible multiphoton microendoscope for label-free imaging in a live animal," Sci. Rep. **5**(1), 18303 (2016).